Plasmonic enhancement of one-photon- and two-photon-excited single-molecule fluorescence by single gold nanorods

Zhang, W.

3

Gold nanorod-enhanced fluorescence enables single-molecule electrochemistry of methylene blue

Redox reactions are central to energy conversion and life metabolism. Here we present electrochemical measurements with fluorescent readout of the redox-sensitive dye Methylene Blue (MB), at the single-molecule (SM) level. To overcome the low fluorescence quantum yield of MB we enhanced fluorescence by individual gold nanorods to achieve the required sensitivity. By measuring the same molecule at different electrochemical potentials we determined the mid-point potential of each single molecule through its redox-induced fluorescence blinking dynamics.

This chapter has been published in Angewandte Chemie International Edition **56**, 13 (2017) [1].

3.1. Introduction

Understanding electrochemical processes is important for a variety of fields such as electrocatalysis [2, 3], nanostructured material synthesis [4, 5], detection of ions [6] and biological processes [7, 8], among others. As redox reactions are extremely sensitive to the local environment, single-molecule (SM) techniques are naturally suited for such studies, since they provide local probes in the subnanometer range, with high sensitivity to changes of the physical and chemical properties of their local surroundings [9]. Electrochemistry with single-molecule sensitivity, proven for the first time by Fan and Bard [10], was an important step towards understanding the environment's influence on electron transfer reactions. An alternative approach to the electrical output is the combination of electrochemical control and optical readout of the molecules involved in the reaction [11]. Such an approach has proved successful with single-molecule sensitivity thanks to surface enhanced Raman spectroscopy (SERS) [12–14]. However, the behavior of molecules in the hot spots responsible for SERS signals is heavily influenced by interactions with the metal, in particular by possible hybridization of molecular orbitals with metal electronic states. Methods for the study of free molecules are thus needed.

Alternatively, fluorescence spectroscopy was also used as a readout of the oxidation or reduction state, relying on the switching of a high quantum yield fluorophore between fluorescent and non-fluorescent states [15]. With this approach, however, SM electrochemical information cannot be accessed due to the fast diffusion of the molecules in solution. Here we worked with immobilized molecules to access millisecond time scales and took advantage of fluorescence enhancement provided by individual gold nanorods (AuNRs) to enable electrochemistry with fluorescence readout at single-molecule level, even for weak emitters. The enhancement factors in the near field of nanorods is much weaker than those in SERS hot spots, but they are felt at much larger distances, of the order of 10 nm, enabling the study of isolated molecules, free from interaction with the metal.

3.2. Results and discussion

We studied the well-known redox-sensitive molecule Methylene Blue (MB), which is widely used for tissue staining [16, 17] and for biochemical studies as a redox indicator [18, 19]. MB is a brightly blue-colored, non-toxic, cationic thiazine dye [20]. MB undergoes the reversible one-proton, two-electron transfer redox reaction shown in Fig. 3.1(a). The product of the reaction is colorless *leuco*-Methylene Blue, which does not absorb visible light [21]. Due to their low quantum yield [22] of $\sim 4\%$ it is difficult to detect single MB molecules by fluorescence. We performed a calibration experiment with MB molecules in solution to estimate the signal from an individual MB molecule and obtained 14 counts s^{-1}, which is well below our detection limit due to dark counts in the detector. Therefore, to achieve SM sensitivity, we propose to employ a fluorescence enhancement scheme.

For this purpose, we used AuNRs with an average size of 40 nm $\times$ 81 nm and a longitudinal surface plasmon resonance at about 660 nm. This plasmon resonance was selected to favor both excitation enhancement, *i.e.*, concentration of the excitation field at the laser wavelength (635 nm) at the tips of the AuNR, and emission enhancement, which depends on the overlap between the emission spectrum of the dye and the plasmon spectrum [23, 24], as

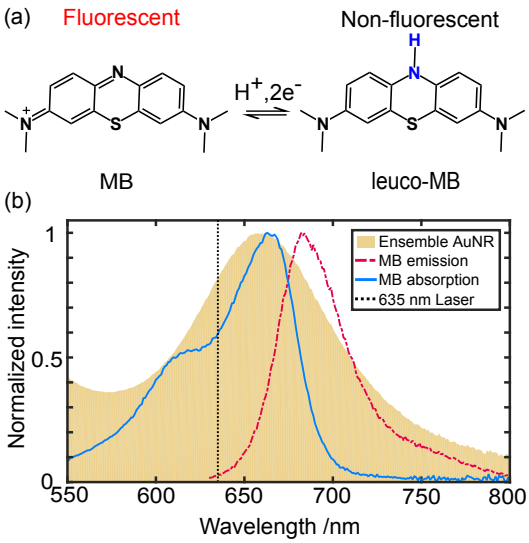

Figure 3.1: (a) Two-electron reduction/oxidation reaction of Methylene Blue (MB). The reduced species, *leuco*-Methylene Blue is non-fluorescent under visible excitation. (b) Absorption (blue) and emission (dashed red) spectra for MB in water. The shaded curve shows the UV-Vis extinction spectrum of a suspension of AuNRs in water. The vertical dotted line shows the wavelength used for fluorescence excitation of MB, on the blue wing of the longitudinal plasmon mode.

can be appreciated for the bulk spectra in Fig. 3.1(b). With these AuNRs we expect enhancement factors as high as 10^3, which will allow detection of SM events above the fluorescence background from unenhanced molecules.

In order to perform electrochemical measurements with fluorescent readout, we used a confocal microscope previously described [25], combined with the electrochemistry setup shown schematically in Fig. 3.2(a). The electrochemical cell presented three electrodes, consisting of a 30-nm thick gold layer deposited on the coverslip with a hole for optical access as the working electrode (WE), a saturated calomel electrode (SCE) as the reference electrode (RE), and a platinum wire as the counter electrode (CE). All the potentials throughout this work were reported relative to SCE. Isolated AuNRs and MB molecules were immobilized on the gold-free area of the coverslip. To allow reliable measurements of SMs, the MB layer had a concentration such that there was on average about 1 molecule in the electromagnetic near field of a AuNR. Because the MB molecules did not have direct electrical contact with the electrodes we used phenazine ethosulfate as an electron mediator to establish the redox potential of the medium surrounding the MB molecules. The working buffer was a pH = 2 HCl-KCl buffer, in which the mid-point potential of phenazine ethosulfate matches that of MB so that the redox potential in the electrochemical cell can be controlled conveniently by the potentiostat. For further details about the experimental configuration and sample preparation, see the Supporting Information.

Firstly, we used the electrochemistry-coupled fluorescence microscope to measure how the fluorescence of a small ensemble of $\sim$ 260 unenhanced molecules immobilized on the glass surface responded to a static redox potential. We applied different potentials and

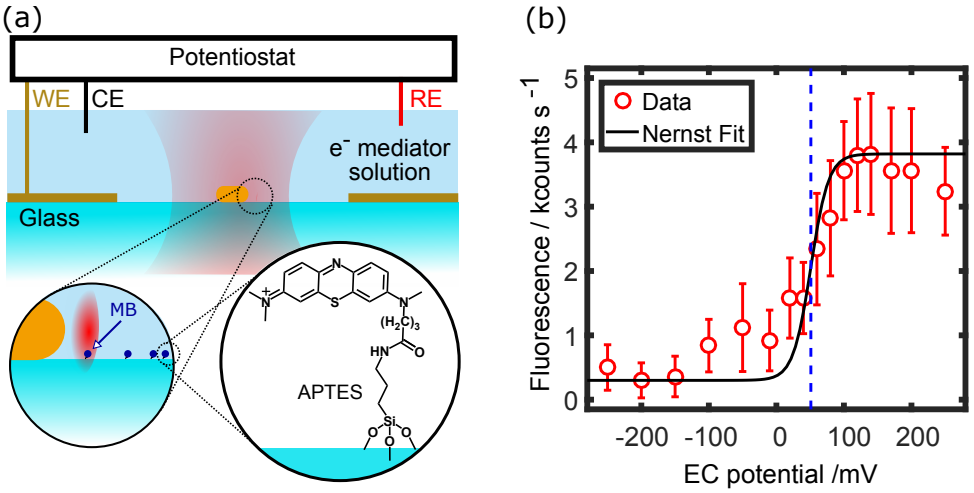

Figure 3.2: Electrochemistry with fluorescent readout. (a) Scheme of the combined electrochemical-confocal setup and sample (WE: working electrode, CE: counterelectrode, RE: reference electrode). Individual AuNRs (not to scale) and MB molecules were immobilized on the glass surface. Phenazine ethosulfate mediates electron transfer between MB molecules and the gold film controlled via the potensiostat. (b) Ensemble fluorescence response of $\sim$ 260 unenhanced MB molecules to the electrochemical potential, showing the controlled switching from the reduced state at low potentials to the oxidized state at high potentials. The black curve is a fit using the Nernst equation and the dashed line illustrates the obtained mid-point potential (51 ± 4 mV).

recorded the corresponding fluorescence counts under 5 W/cm^2 illumination once the equilibrium was established. Figure 3.2(b) shows the intensity measured as a function of the applied voltage, where the switching of MB molecules from the dark to the bright state can be seen. We assign the hump at around -50 mV to molecule-substrate interactions, as it was not observed when doing the same measurement with MB solutions (data not shown). We modeled the ensemble of MB molecules with the Nernst equation (see the Supporting Information) and obtained a mid-point potential of 51 ± 4 mV. This shows our capability of performing electrochemical experiments through fluorescence monitoring of a small ensemble.

Secondly, we turned to SM experiments, which are possible thanks to the enhancement provided by the AuNRs. We worked in the situation presented in Fig. 3.2(a), with one molecule in the near-field of the AuNR and several molecules in the confocal volume, contributing to the total signal. The low QY of MB has the advantage of providing a low background from those unenhanced molecules which does not obscure the signal from the enhanced molecule, *i.e.*, the signal from the enhanced molecule is high compared to the background. At SM level we expect to see fluorescence blinking induced by the dynamic equilibrium of the redox reaction. When the potential is set to the mid-point potential, we expect the molecule to spend half of the time reduced and half of the time oxidized, which will be evidenced by equal on- and off-times for the blinking. With the same reasoning, for reducing (oxidizing) potentials we expect that the molecule will spend more time in the off (on) state.

The fluorescence time trace of a single enhanced MB molecule is shown in Fig. 3.3(a),

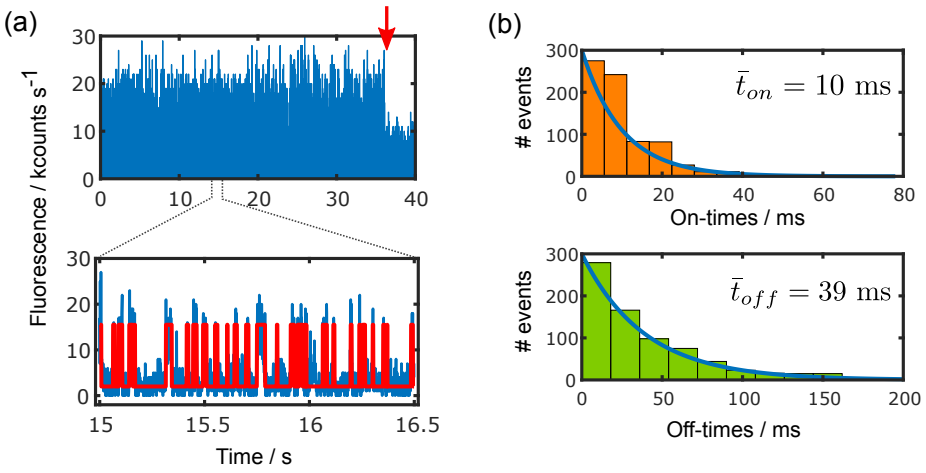

Figure 3.3: Single-molecule measurements at a fixed potential. (a) (top) Fluorescent time trace from a AuNR-enhanced single molecule (binned to 1 ms) under an electrochemical potential of 80 mV. The arrow shows the one-step bleaching event. (bottom) Expansion that evidences the blinking behavior. The red trace was obtained through a step-detection algorithm. For this particular SM we estimated an enhancement factor value of $\sim$ 800. (b) Blinking events histograms for the on- (top) and off-times (bottom), showing an exponential distribution. The estimated mean times from single-exponential fits (blue solid lines) are shown on each plot.

where SM reduction and oxidation events can be clearly distinguished, as well as a single-step bleaching event. The laser excitation peak intensity was 5 W/cm^2 . The bin time of 1 ms was chosen so that the on/off states can be clearly observed (for further discussion on this point, refer to the Supporting Information). A step-detection algorithm [26] was used to extract the times associated to the switching events, shown in the figure in red. The obtained on- and off-times follow an exponential distribution with mean on- and off-times of $\bar{t}_{\text{on}} = 10.0 \pm 0.7$ ms and $\bar{t}_{\text{off}} = 39 \pm 2$ ms.

We further studied the blinking behavior of the *same* molecule at different electrochemical potentials. We detected the enhanced fluorescence from the same single molecules at different potentials successively under the same illumination conditions as before. Figure 3.4a shows three time traces (binned to 1 ms) obtained from such a molecule, where the blinking dynamics is evidently responding to the electrochemical potential. The comparison of the traces shows that the on-time increases when the potential is increased while the off-time decreases, in accordance with the expected behavior. This general trend is observed in all the studied molecules.

To model the electrochemical switching of single molecules more quantitatively, we used the Nernst equation:

$$E = E_0 + \frac{k_{\text{B}}T}{ne} \ln\left(\frac{\bar{t}_{\text{on}}}{\bar{t}_{\text{off}}}\right) , \tag{3.1}$$

where E is the applied potential, E_0 the mid-point potential, k_{B} the Boltzmann constant, T the absolute ambient temperature, n the number of electrons involved in the reaction, e the electron charge and $\bar{t}_{\text{on}}$, $\bar{t}_{\text{off}}$ the mean on and off blinking times. Figure 3.4(b) shows several

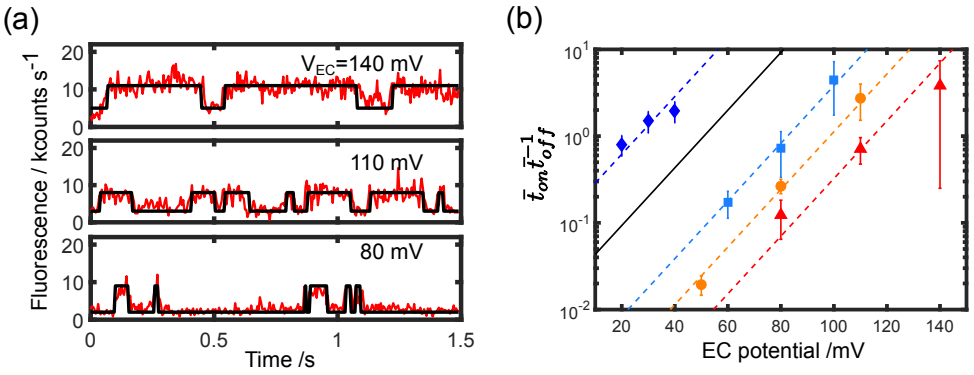

Figure 3.4: SM electrochemistry with fluorescence readout. (a) Fluorescence time traces of the same single molecule at different potentials, where different blinking dynamics can be seen. (b) The ratio $\bar{t}_{\rm on}/\bar{t}_{\rm off}$ is plotted as a function of the potential for some measured single molecules. Different symbols and colors represent different molecules. The red triangles correspond to the traces in a). The dashed lines are fits using the Nernst equation to extract the mid-point potential E_0 for each molecule, while the black solid line corresponds to the ensemble mid-point value extracted from data in Fig. 3.2(b).

$\bar{t}_{\rm on}/\bar{t}_{\rm off}$ values (symbols) and fits with the Nernst equation to obtain E_0 (dotted lines). The measured distribution of mid-point potentials for single molecules can be modeled by a Gaussian with a central value of $\langle E_0^{\rm SM}\rangle = 78.3 \pm 0.1$ mV and a dispersion of $\sigma^{\rm SM} = 21.1 \pm 0.1$ mV (see Fig. S3.5).

The average SM mid-point potential is significantly higher than the ensemble value for the laser intensity used (51 mV, see Fig. 3.2(b). To address this discrepancy, we performed the same ensemble measurements as in Fig. 3.2(b) with varying excitation intensities and observed a clear increase in mid-point potential with increasing intensity (see Fig. S3.6). This presents a possible explanation for the mentioned shift in the average mid-point potential: a molecule in the vicinity of the AuNR is excited by an enhanced field that can be as high as 300-fold [24], therefore the expected mid-point potential for such a molecule will be shifted to higher values by the strong irradiation. In order to further support this interpretation, we performed power dependence measurements on single molecules, shown in Fig. S3.7. We found that the same molecule shows higher mid-point potential when excited at higher intensity (see Fig. S3.7(a)), supporting further that laser irradiation has some influence on the redox reaction. A quantitative characterization and a mechanistic study of this photo-induced redox reaction require more experimental and theoretical work.

3.3. Conclusions

In conclusion, we have presented a scheme to study electrochemical properties of Methylene Blue at single-molecule level using fluorescence readout. Despite the low quantum yield of MB we were able to detect SM fluorescence blinking due to the high enhancement factors given by individual gold nanorods. Our single-molecule study of the *same* molecule at different redox potentials reveals that a single molecule's fluorescence emission responds to the ambient redox potential according to the Nernst equation, albeit the effective mid-point potential may be altered by the probing light. Our technique could be applied to measure the

local redox potential in chemical or biological systems by single molecules and opens up the possibility of single-molecule electrochemical studies of a broader set of weakly fluorescent molecules.

3.4. Supporting information

3.4.1. Experimental setup

Combined electrochemical-optical measurements

The optical setup for fluorescence microscopy was described previously [27]. Briefly, fluorescence images and single-molecule fluorescence intensity trajectories were recorded using a home-built sample-scanning confocal microscope, equipped with an oil immersion objective (100×, NA=1.4, Zeiss), an avalanche photodiode (APD, SPCM-AQR-14, PerkinElmer) and time-correlated single-photon counting (TCSPC) electronics (Timeharp 200, PicoQuant). A 635 nm pulsed laser (LDH-P-C-635B, PicoQuant) was used for exciting the dye. A 532 nm Nd:YAG laser was used to measure the photoluminescence spectra of AuNRs, which closely resemble their scattering spectra [28]. These photoluminescence spectra were used to confirm that the nanostructure in use was an individual nanorod, which has a well-defined near-field intensity distribution.

All electrochemical experiments were carried out in a specially-designed electrochemical cell that fits the microscope. It has a gold wire connected to the gold film on the glass coverslip as the working electrode, a saturated calomel electrode as the reference electrode, a platinum wire coil as the counter electrode (see Fig.3.2(a) in the main text) and is controlled by a potentiostat (CHI832B, CH Instrument). The working solution was 100 μM phenazine ethosulfate (PES, Santa Cruz Biotechnology) dissolved in a KCl-HCl buffer (pH = 2.0, 50 mM KCl). The solution (5 mL) was inside a Teflon tube and supported by the glass sample.

Controlling the redox potential

We used the potentiostat and PES (mid-point potential E_0 = 67 mV *vs.* saturated calomel electrode at pH = 2) as an electron mediator to control the redox potential around Methylene Blue molecules. PES in the oxidized state (PES_{ox}) may receive electrons from the electrode and get reduced to PES_{red}. MB molecules studied in the experiment were very close (within 40 μm) to the working electrode (which is the gold film) [29]. In this close vicinity of the working electrode, the redox potential is controlled by the concentration ratio of $[PES_{ox}]/[PES_{red}]$, which in turn is determined by the electrical potential applied on the gold film *via* the Nernst equation. In this way, through the redox equilibrium between PES and MB, the redox potential around MB was controlled by the potential applied to the working electrode.

Since the establishment of the redox potential relies on the diffusion of the electron mediator, the actual redox potential sensed by an MB molecule is dependent on the time after an external electrical potential is applied as well as on its distance to the working electrode. In our experiments, we waited long enough time (at least 2 minutes) after applying a new potential and measured only molecules close to (within 40 μm) the edge of the gold film electrode. In this way, the measured molecules were in a redox potential which is close enough to the electrical potential applied to the gold working electrode. To test this idea

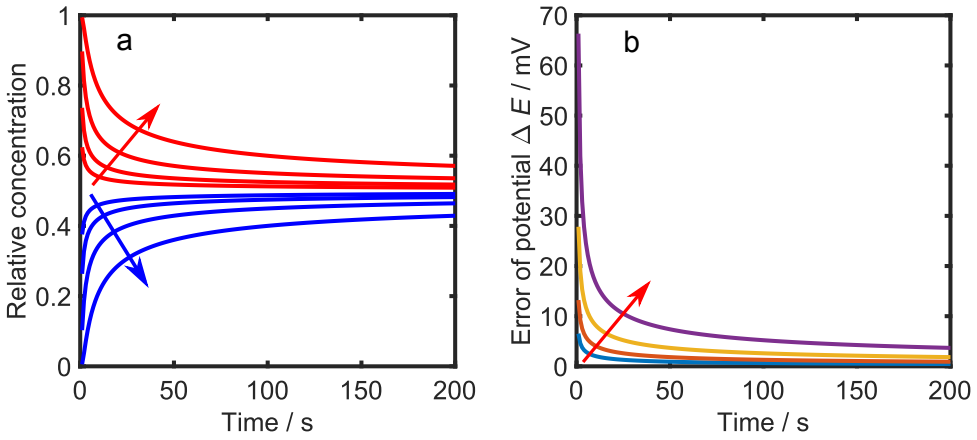

Figure S3.1: Control of the redox potential relies on the diffusion of the electron mediator. a) Calculated concentration evolution at positions with different distances to the electrode (10 μm, 20 μm, 40 μm and 80 μm) after the mid-point potential is applied at t = 0 to a solution of PES_{ox}. The arrows indicate increasing distance. The concentrations of oxidized (red) and reduced (blue) PES are scaled by the original concentration of PES_{ox}. b) Calculated error of redox potential compared to the applied potential at different distances away from the electrode (10 μm, 20 μm, 40 μm and 80 μm) after the mid-point potential is applied at t = 0. The arrow indicates increasing distance. The diffusion coefficient of PES in the aqueous buffer is assumed to be $5 \times 10^{-6}\mathrm{cm}^2/\mathrm{s}$ in the calculations.

more quantitatively, we assumed that the mid-point potential of PES (67 mV) is applied to a solution of PES_{ox} at $t = 0$. PES_{ox} will be reduced on the electrode surface and the concentration ratio of $[PES_{ox}]/[PES_{red}]$ on the electrode surface will immediately be 1. We calculated the time evolution of $[PES_{ox}]$ (red) and $[PES_{red}]$ (blue) near the working electrode using a linear diffusion model [29] (Fig. S3.1(a)). We see that $[PES_{ox}]$ decreases while $[PES_{red}]$ increases because $[PES_{red}]$ generated on the electrode surface diffuses into the solution. $[PES_{ox}]/[PES_{red}]$ is approaching 1 over time, namely, the local redox potential is approaching 67 mV. Moreover, the local redox potential at closer distance to the electrode surface goes faster to the applied potential. We further estimated the error of the local redox potential compared to the applied potential (Fig. S3.1(b)) using

$$\Delta E = \frac{59.2\ \mathrm{mV}}{2} \log_{10} \frac{[\mathrm{PES_{ox}}]}{[\mathrm{PES_{red}}]}, \tag{3.2}$$

since 2 electrons are involved in the redox reaction. Figure S3.1b shows, for instance, that 100 s after the potential is applied, the redox potential 40 μm away from the electrode is only 2.60 mV higher than the applied potential. Therefore in our experiment we used the applied potential as the redox potential around the MB molecules.

3.4.2. Sample preparation

Gold nanorod immobilization. The average dimension of the gold nanorods (AuNRs) was 40 nm $\times$ 81 nm according to the manufacturer (Nanoseedz). The concentration of hexadecyl-trimethyl-ammonium bromide (CTAB) in the nanorod suspension was reduced

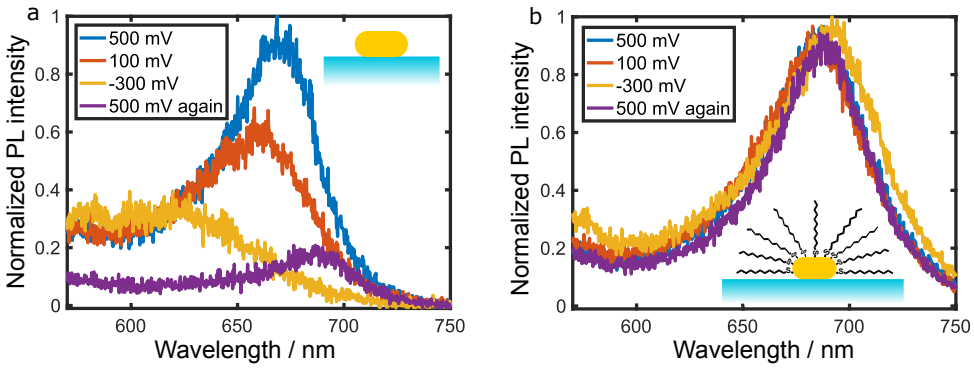

Figure S3.2: a) The PL spectra of a single bare AuNR (shown schematically in the inset) at different electrochemical potentials. The spectral changes took place within a few seconds after a new potential was applied. b) The PL spectra of a coated AuNR (shown schematically in the inset, not to scale) at different electrochemical potentials. No significant spectral changes of AuNRs could be observed after passivation.

by centrifugation and resuspension in Milli-Q water to less than 10 μM to ensure successful immobilization. Number 1 glass coverslips (Menzel-Gläser, ϕ = 25 mm) were used for all immobilizations. The coverslips were sonicated in water (20 min) and ethanol (20 min). They were then dried with a clean nitrogen flow and cleaned with ultraviolet-ozone cleaner (model 42-220, Jelight) for 30 minutes for the next step or stored in ethanol. AuNRs were immobilized on the coverslip by spin-coating from the water suspension. After that, the remaining CTAB was removed by rinsing with MilliQ water and treating with UV/Ozone for 30 minutes. The AuNRs are well isolated on the slide with a density of $\sim$10 nanorods per 100 μm^2. Approximately 90% of the identified bright spots were measured to be single nanorods while the others stemmed from aggregates of nanorods. For SM measurements, we were only interested in molecules in the vicinity of single AuNRs, whose electromagnetic near-field is well-defined.

Gold nanorod coating. It was found experimentally that bare AuNRs were not stable during electrochemical measurements, as is evidenced by the spectral change of the AuNRs (Fig. S3.2(a)). A few seconds after the electrochemical potential was changed the photoluminescence (PL) spectrum of the AuNR shifted and the PL brightness decreased. These changes were irreversible. This issue might be the consequence of dissolution by phenazine ethosulfate when the potential is changed. Similar irreversible particle reshaping phenomena in electrochemistry experiments were reported by previous researchers [30, 31]. In order to protect the AuNRs, saturated aliphatic chains were compactly functionalized on them so that they are isolated from the ambient solution (see the inset of Fig. S3.2(b)). Experimentally, the coverslips with AuNRs were treated with a 10 mM 1-undecanethiol ($CH_3(CH_2)_{10}SH$, Sigma-Aldrich) solution in 2-propanol (Sigma-Aldrich) overnight at room temperature. The slides were then rinsed extensively with 2-propanol and dried with nitrogen. Once the AuNRs were coated in this manner, we did not observe any etching or reshaping throughout our experiments (see Fig. S3.2(b)).

Silanization of the coverslips. The coverslips with coated AuNRs were then immersed

for 30 minutes with gentle stirring in a methanol solution containing 1% (3-Aminopropyl)triethoxysilane (APTES, Sigma-Aldrich) and 5% glacial acetic acid. Thereafter, the silanized slides were washed thoroughly with methanol and ethanol and dried with a nitrogen flow [32]. If not immediately used for the next step, they were stored inside a desiccator to maintain the activity of the amine groups.

Gold film sputtering. A small piece of clean glass slide (a few mm) was put at the center of every coverslip before any film was sputtered. A 2-nm-thick adhesion layer of molybdenum-germanium (MoGe) film was deposited onto the coverslips by magnetron sputtering (Z-400 system, Leybold). A 30-nm-thick gold film was immediately sputtered onto the slides in the same system. The thicknesses were estimated from the deposition rates (5.5 nm/min for MoGe and 15.2 nm/min for Au in a $<6 \times 10^{-6}$ mbar Argon environment) and times. Afterwards, the slides were taken out of the sputtering system and the small glass pieces were blown away. There were no MoGe or Au films in the area blocked by the tiny glass. Amine groups in this area were still exposed and active for immobilizing MB molecules.

Immobilization of MB molecules. Next the coverslip was placed into a circular sample holder. 1 mL solution of 300 nM MB with a N-Hydroxysuccinimide ester (NHS-ester) substituent (ATTO-TEC GmbH) in 0.1 M phosphate buffer (pH = 7.6) was applied to the coverslip. NHS-ester reacts readily with the amine groups on the coverslip to form stable amide bonds, and MB molecules thus are immobilized (depicted in Fig. S3.3). In order to accurately control the surface density of MB molecules the immobilization process was monitored *in situ*. Experimentally, the coverslip was mounted on the confocal setup and the surface close to the gold film was imaged every few minutes with the 635-nm laser. The intensity of the laser was kept low ($\sim$5 W/cm^2) to minimize photobleaching. The effective confocal volume of the optical setup was measured in a separate experiment to be 0.3 fL. With this information the count rate from an individual MB molecule was obtained by measuring the brightness of a MB NHS-ester solution of known concentration. The number of molecules per unit area was then estimated by dividing the brightness of the immobilized MB molecules by the count rate per molecule, assuming that the brightness of MB molecules does not change upon binding to the glass surface. The target molecular density is such that there is on average 1 molecule in the near-field of a AuNR. The area of the near-field in the plane of the substrate was estimated to be 40 nm$\times$20 nm$\times$2 = 1600 nm^2 considering the dimension of the AuNR. One molecule in this area corresponds to 177 molecules in the diffraction limited confocal area ($\sim$300 nm in radius). In practice, some AuNRs might have more than 1 molecule nearby but we only considered single molecules indicated by clear two-level blinking. Once the desired number of molecules is obtained, the reaction was terminated by removing the solution of MB NHS-ester. The slide was then washed several times with HCl-KCl buffer (pH = 2.0) and immediately used for electrochemistry-coupled single-molecule measurements.

3.4.3. Modeling the ensemble response to the potential

In this section we model the fluorescence response of an ensemble of $\sim$260 molecules in the focal area to the potential. The mean intensity I_m emitted by each molecule over several

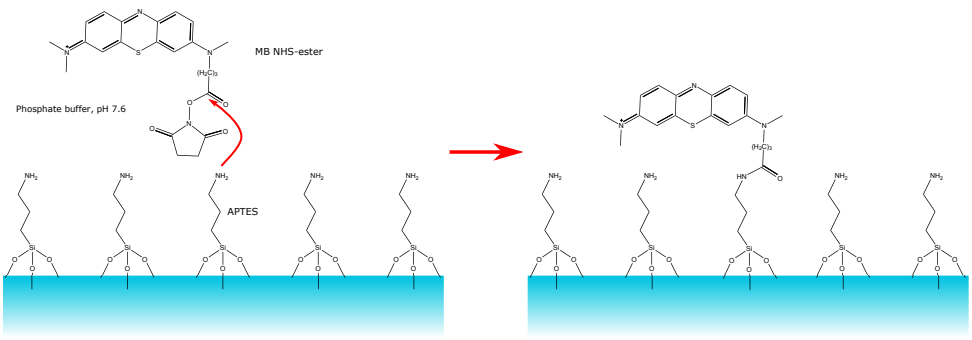

Figure S3.3: MB with a NHS-ester substituent is reacted with APTES silanized on the slide resulting in a covalent amide bond formation.

switching cycles can be calculated as

$$I_m = \langle I(t) \rangle_t = B + I_{\text{on}}^{SM} \frac{\bar{t}_{\text{on}}}{\bar{t}_{\text{on}} + \bar{t}_{\text{off}}} , \tag{3.3}$$

where $\langle I(t) \rangle_t$ indicates time average, B is the background intensity (200 counts s^{-1}), $I_{\text{on}}^{\text{SM}}$ is the on-intensity for one molecule and $\bar{t}_{\text{on}}$ and $\bar{t}_{\text{off}}$ are the mean on- and off-times, respectively. Since the blinking comes from the redox reaction of MB, the ratio of on- and off-times can be expressed using the Nerst equation

$$\frac{\bar{t}_{\text{off}}}{\bar{t}_{\text{on}}} = \exp\left(\frac{E_0 - V}{\alpha}\right) , \tag{3.4}$$

where V is the applied potential, E_0 the mid-point potential and $\alpha = \frac{k_{\text{B}}T}{ne} \approx 13$ mV.

If we assume a probability density function (PDF) $g(\zeta)$ for mid-point potentials and that all the molecules contribute with the same intensity, we can estimate the ensemble intensity distribution summing all the contributions from each single-molecule I_m weighted by this distribution:

$$\langle I_m \rangle_e (V) = B + I_{\text{on}} \int \frac{g(\zeta)}{1 + \exp(\frac{\zeta - V}{\alpha})} \text{d}\zeta , \tag{3.5}$$

where $\langle I_m \rangle_e$ indicates ensemble averaging, B is the background signal and $I_{\text{on}} = N_{\text{molec}} I_{\text{on}}^{\text{SM}}$. The simplest model would be to have a single mid-point potential value, $\bar{E}_0$, in which case the PDF is a delta function $\delta(\zeta - \bar{E}_0)$. We fitted this simple model to our experimental data (Fig. 3.2(b) in the main text) and obtained $\bar{E}_0 = 51 \pm 4$ mV.

3.4.4. Blinking time scales

In order to extract the characteristic times associated with the fluorescence emission of SMs we calculated the autocorrelation function and found two components with clearly separated time scales as shown in Fig. S3.4. The short component ($\tau_s = 135.9 \pm 21.5$ μs) may be

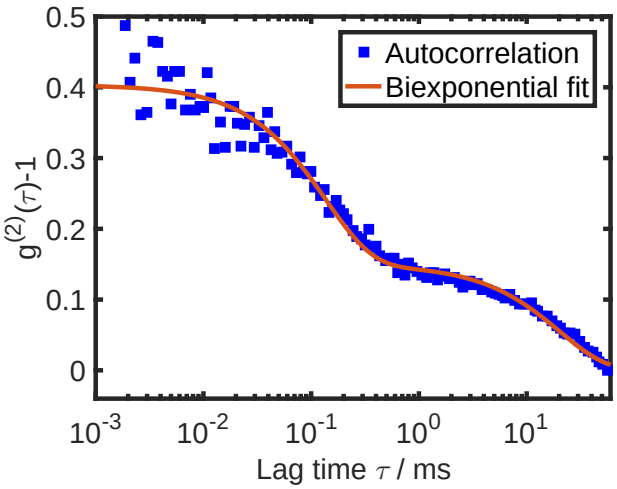

Figure S3.4: Autocorrelation traces (blue dots) measured on a AuNR-enhanced MB molecule at 120 mV with biexponential fit (red curve). The distinct short and long correlation times correspond to blinking from the triplet state and redox-induced blinking, respectively.

attributed to blinking from the triplet state as it is close to the reported triplet lifetime of MB [33]. The long component ($\tau_L = 20.3 \pm 4.6$ ms) is attributed to redox-induced blinking since the order of magnitude of this component is in the range expected for the redox reaction of MB [34, 35]. The well separated time scales allowed us to work with 1ms-binned time traces to study only the redox-induced intensity fluctuations.

3.4.5. Histogram of single-molecule mid-point potentials

In Fig. S3.5 we show the histogram of mid-point potentials for single molecules. By modeling the distribution with a Gaussian shape we get a central value of $\left\langle E_0^{\mathrm{SM}} \right\rangle = 78.3 \pm 0.1$ mV and a dispersion of $\sigma^{\mathrm{SM}} = (21.1 \pm 0.1)$ mV.

3.4.6. Dependence of the electrochemical reaction on the laser intensity

Intensity dependence of a small ensemble

To gain more insight into the dependence of MB's redox properties on laser intensity, we carried out the same ensemble measurement as shown in Fig. 3.2(b) in the main text with different excitation intensities. Ensemble-averaged mid-point potentials ($\bar{E}_0$) were obtained for each case and plotted against laser intensity in Fig. S3.6. Likewise, the figure shows that generally higher $\bar{E}_0$ values are observed if higher laser intensities were used. When the intensity is decreased, the intensity dependence of $\bar{E}_0$ reaches a plateau, where the redox state of molecules is independent of the excitation laser intensity. For a more quantitative analysis we fitted the data with a saturation curve, $\bar{E}_0(I) = E_0^{\mathrm{dark}} + C\frac{I/I_s}{1+I/I_s}$, where C is a proportionality constant, Is the saturation value and E_0^{dark} the mid-point potential in the

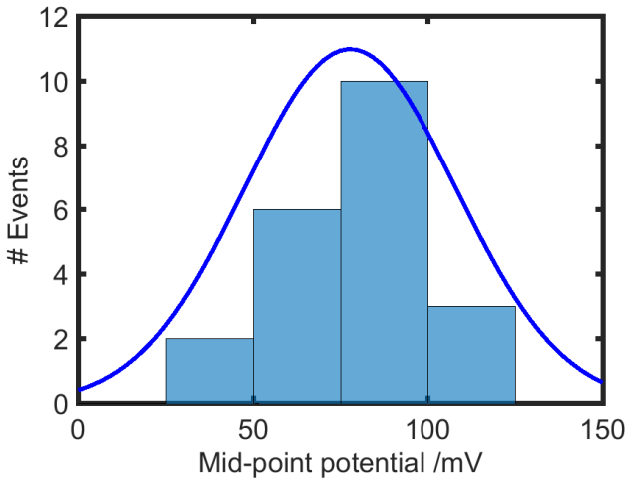

Figure S3.5: Histogram of mid-point potentials for 22 single molecules with the estimated probability distribution function with a Gaussian shape (blue solid curve).

absence of light. It is unclear to us why the two points at high intensities strongly deviate from the fit, unless this is a consequence of fast photobleaching at high intensities.

Intensity dependence of single molecules
Fluorescence emission from AuNR-enhanced single MB molecules was recorded with different excitation intensities under a fixed potential of 80 mV. Three time traces from an example molecule shown in Fig. S3.7(a) clearly evidence the dependence of oxidation/reduction dynamics on the excitation intensity. Investigation of more SMs reveals that AuNR-enhanced molecules show higher mid-point potentials under excitation of higher intensity. The intensity dependence of the measured mid-point potential is possibly a consequence of photo-induced reduction taking place in the triplet state of MB, since MB can be photo-excited to the long-lived triplet state ($\tau_{\mathrm{T}} = 450\ \mu$s) with high probability (triplet quantum yield $\phi_{\mathrm{T}} = 0.52$) [33]. This hypothesis is supported by Fig. S3.7(b), which shows that the reduction rate ($\bar{t}_{\mathrm{on}}^{-1}$) of SMs is increased by increasing the excitation intensity. The oxidation rate ($\bar{t}_{\mathrm{off}}^{-1}$), on the other hand, is independent of laser intensity as *leuco*-MB does not absorb visible light. Consequently, measured mid-point potentials of SMs are positively correlated with the laser intensity. Therefore, the on- and off-time analysis of SM fluorescence of MB overestimates the local redox potential.

3.4.7. Fluorescence enhancement analysis

The AuNR antenna in the vicinity of a MB molecule leads to fluorescence enhancement by two main mechanisms, excitation enhancement and emission enhancement. The former one arises from the high concentration of electric field at the tips of the nanorod. When a molecule is placed inside this hot spot, the local intensity can be as high as 300 times the input laser intensity, leading to an increased excitation rate. The latter enhancement mech-

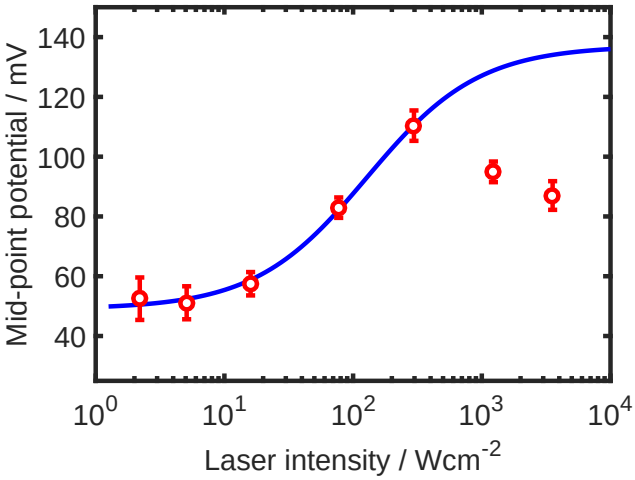

Figure S3.6: The average mid-point potential ($\bar{E}_0$) for a small ensemble depends on the laser intensity that is used for measuring. The blue is a fit according to a saturation behavior as described in the text.

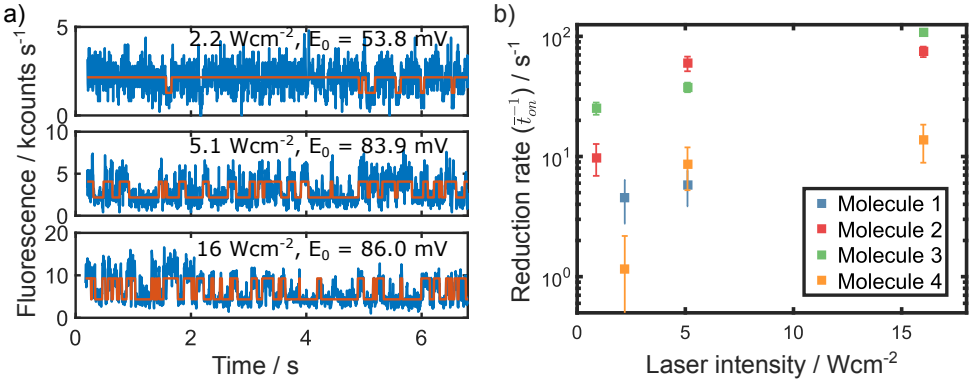

Figure S3.7: a) Fluorescence time traces recorded on the same molecule under 80 mV excited with different laser intensities. The molecule behaves differently at different excitation intensities. The red curves indicate the identified on/off state transitions. b) Reduction rates ($\bar{t}_{\mathrm{on}}^{-1}$) of four different single molecules (distinguished by different colors) under 80 mV at different laser intensities. We see a general correlation between higher reduction rate and higher intensity. Molecule 4 shown in yellow is less light-sensitive and corresponds to the molecule presented in a).

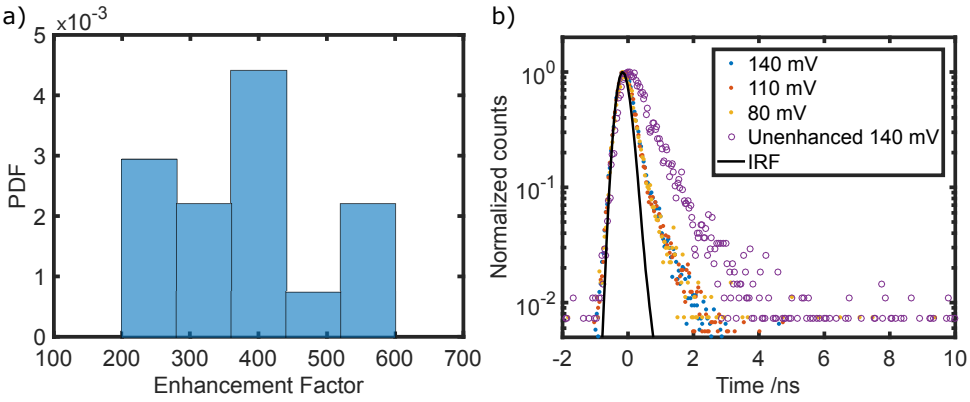

Figure S3.8: a) Total enhancement factor histogram for the 22 single molecules presented in Fig. S3.5. b) Lifetime curves for a small ensemble of unenhanced MB molecules, with a lifetime of 670 ps (open circles) and SM lifetimes for different EC potentials noted in the legend (dots). The black curve shows the IRF for our system. The enhanced lifetime remained at 360 ps regardless the applied EC potential.

anism is related to the change in the radiative and nonradiative decay rates of the molecule and depends on the distance, position, and orientation of the molecular dipole moment with respect to the local field around the AuNR and on the spectral overlap between the emitter and the nanorod [24]. We chose our AuNR sample to maximaze the overlap with the emission of MB. Regarding the dipolar orientation, due to the flexibility of the bonds that attach the MB molecules to the glass substrate, the molecules may rotationally diffuse at the end of their tether. The expected time scale for that diffusion is in the nanosecond range which is faster than any other process of interest here, so we may be observing an average of all the posible orientations. However, such process would not affect the reported values for the electrochemical quantities. Similarly, if the molecules are stuck to the surface, their orientation would be constant or vary slowly and thus would not alter the measured dynamics.

Fig. S3.8(a) shows a histogram of the total enhancement factor obtained from the SM time traces measured for this work. The enhancement factors vary from 200 to 600, a reasonable set of values for the nanorods we are using. We attribute the dispersion in values to the stochastic positioning of the molecules in the vicinity of the nanorod as well as the molecular orientation. Fig. S3.8(b) shows the comparison of the lifetime for unenhanced MB molecules and the enhanced SM data for different applied EC potentials, where a reduction in lifetime of ≈ 1.9 was measured. Notably, the lifetime is not influenced by the applied EC potential. We also show the instrument response function as a solid line.

3.4.8. Scatter plots

From our experimental data we can also extract information about correlations between the relevant parameters of the system. Firstly we look for correlations between the SM midpoint potential and the fluorescence enhancement factor. The scatter plot in Fig. S3.9 shows a positive correlation between these quantities, which is consistent with our interpretation

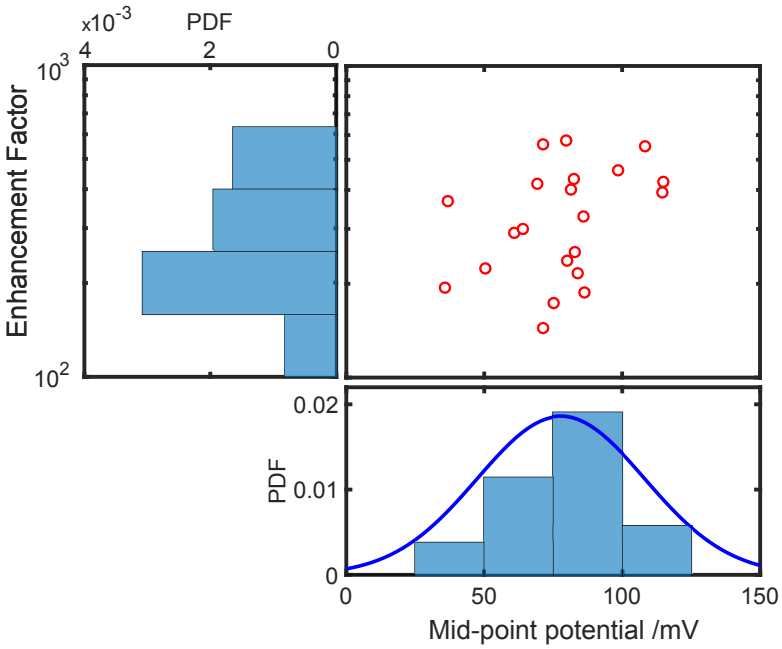

Figure S3.9: Enhancement factor as a function of measured mid-point potential at single-molecule level. Each dot in the scatter plot corresponds to one molecule. The histograms for each quantity are also shown.

of the high average mid-point potential for single molecules due to the near-field laser field. Using the data in Fig. S3.6 and the observed value $\langle E_0^{\mathrm{SM}} \rangle = 78.3$ mV we may estimate the average intensity felt by the molecules in the near field around 100 W cm^{-2}, which is a reasonable expectation value.

Secondly, we look for correlations between the mid-point potential and the enhanced fluorescence lifetime. The natural lifetime of a small ensemble MB molecules was measured to be 670 ps and due to the presence of the nanorod this lifetime is reduced. Figure S3.10 shows the scatter plot of the measured lifetime for each single molecule presented in the paper as a function of the mid-point potential. Also a histogram of lifetimes is shown. In this case no clear correlation is found between these two parameters suggesting that the electrochemical properties are not affected by a change in the population of the excited state of MB.

Finally, we correlated the single-molecule lifetime and the enhancement factors measured, as shown in the scatter plot from Fig. S3.11. As it was previously shown some degree of correlation is found since higher total enhancement factors are achieved when the lifetime reduction is stronger [24].

References

[1] W. Zhang, M. Caldarola, B. Pradhan, and M. Orrit, *Gold nanorod enhanced fluorescence enables single-molecule electrochemistry of methylene blue,* Angewandte

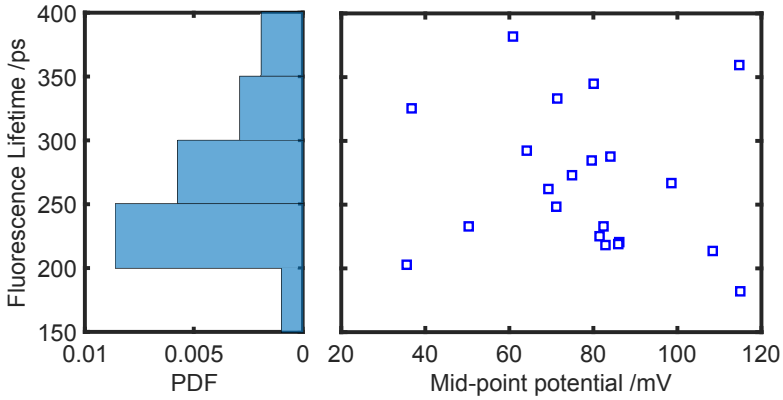

Figure S3.10: Single-molecule fluorescence lifetime as a function of measured mid-point potential. Each dot in the scatter plot corresponds to one molecule. No clear correlation is observed.

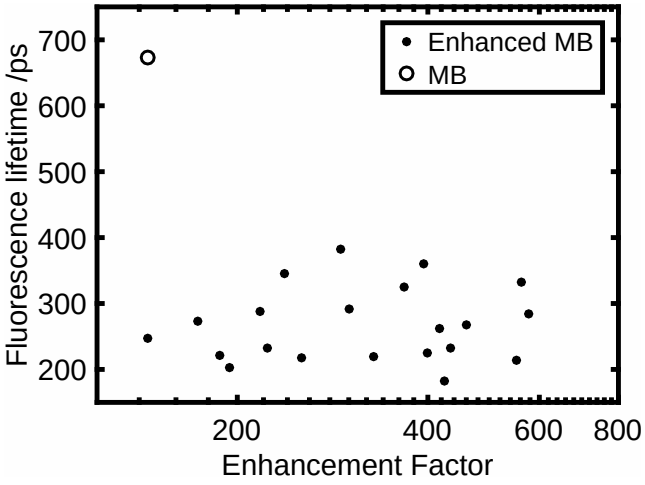

Figure S3.11: Single-molecule fluorescence lifetime vs enhancement factor. Each dot in the scatter plot corresponds to one molecule and some correlation is found between these quantities, as expected. The open circle corresponds to the unenhanced lifetime, shown for reference.

Chemie International Edition **56**, 3566 (2017).

[2] X. Mao and T. A. Hatton, *Recent advances in electrocatalytic reduction of carbon dioxide using metal-free catalysts,* Industrial & Engineering Chemistry Research **54**, 4033 (2015).

[3] M. T. Koper, *Structure sensitivity and nanoscale effects in electrocatalysis,* Nanoscale **3**, 2054 (2011).

[4] Y.-Y. Yu, S.-S. Chang, C.-L. Lee, and C. C. Wang, *Gold nanorods: electrochemical synthesis and optical properties,* The Journal of Physical Chemistry B **101**, 6661 (1997).

[5] G.-R. Li, H. Xu, X.-F. Lu, J.-X. Feng, Y.-X. Tong, and C.-Y. Su, *Electrochemical synthesis of nanostructured materials for electrochemical energy conversion and storage,* Nanoscale **5**, 4056 (2013).

[6] C. P. Byers, B. S. Hoener, W.-S. Chang, S. Link, and C. F. Landes, *Single-particle plasmon voltammetry (spPV) for detecting anion adsorption,* Nano Letters , 2314 (2016).

[7] R. H. Goldsmith, L. C. Tabares, D. Kostrz, C. Dennison, T. J. Aartsma, G. W. Canters, and W. Moerner, *Redox cycling and kinetic analysis of single molecules of solution-phase nitrite reductase,* Proceedings of the National Academy of Sciences **108**, 17269 (2011).

[8] J. M. Salverda, A. V. Patil, G. Mizzon, S. Kuznetsova, G. Zauner, N. Akkilic, G. W. Canters, J. J. Davis, H. A. Heering, and T. J. Aartsma, *Fluorescent cyclic voltammetry of immobilized azurin: direct observation of thermodynamic and kinetic heterogeneity,* Angewandte Chemie International Edition **49**, 5776 (2010).

[9] S. G. Lemay, S. Kang, K. Mathwig, and P. S. Singh, *Single-molecule electrochemistry: present status and outlook,* Accounts of Chemical Research **46**, 369 (2012).

[10] F.-R. F. Fan and A. J. Bard, *Electrochemical detection of single molecules,* Science **267**, 871 (1995).

[11] C. M. Hill, D. A. Clayton, and S. Pan, *Combined optical and electrochemical methods for studying electrochemistry at the single molecule and single particle level: recent progress and perspectives,* Physical Chemistry Chemical Physics **15**, 20797 (2013).

[12] E. Cortés, P. G. Etchegoin, E. C. Le Ru, A. Fainstein, M. E. Vela, and R. C. Salvarezza, *Monitoring the electrochemistry of single molecules by surface-enhanced raman spectroscopy,* Journal of the American Chemical Society **132**, 18034 (2010).

[13] E. Cortés, P. G. Etchegoin, E. C. Le Ru, A. Fainstein, M. E. Vela, and R. C. Salvarezza, *Strong correlation between molecular configurations and charge-transfer processes probed at the single-molecule level by surface-enhanced raman scattering,* Journal of the American Chemical Society **135**, 2809 (2013).

[14] S. Zaleski, M. F. Cardinal, J. M. Klingsporn, and R. P. Van Duyne, *Observing single, heterogeneous, one-electron transfer reactions,* The Journal of Physical Chemistry C **119**, 28226 (2015).

[15] C. Lei, D. Hu, and E. J. Ackerman, *Single-molecule fluorescence spectroelectrochemistry of cresyl violet,* Chemical Communications , 5490 (2008).

[16] M. I. F. Canto, S. Setrakian, R. E. Petras, E. Blades, A. Chak, and M. V. Sivak, *Methylene blue selectively stains intestinal metaplasia in barrett's esophagus,* Gastrointestinal Endoscopy **44**, 1 (1996).

[17] M. Wainwright and K. Crossley, *Methylene blue-a therapeutic dye for all seasons?* Journal of Chemotherapy **14**, 431 (2002).

[18] K. Kerman, D. Ozkan, P. Kara, B. Meric, J. J. Gooding, and M. Ozsoz, *Voltammetric determination of DNA hybridization using methylene blue and self-assembled alkanethiol monolayer on gold electrodes,* Analytica Chimica Acta **462**, 39 (2002).

[19] E. Farjami, L. Clima, K. V. Gothelf, and E. E. Ferapontova, *DNA interactions with a methylene blue redox indicator depend on the DNA length and are sequence specific,* Analyst **135**, 1443 (2010).

[20] L. Michaelis and S. Granick, *Metachromasy of basic dyestuffs,* Journal of the American Chemical Society **67**, 1212 (1945).

[21] N. R. de Tacconi, J. Carmona, and K. Rajeshwar, *Reversibility of photoelectrochromism at the TiO_2/methylene blue interface,* Journal of the Electrochemical Society **144**, 2486 (1997).

[22] J. Olmsted, *Calorimetric determinations of absolute fluorescence quantum yields,* The Journal of Physical Chemistry **83**, 2581 (1979).

[23] D. Punj, J. de Torres, H. Rigneault, and J. Wenger, *Gold nanoparticles for enhanced single molecule fluorescence analysis at micromolar concentration,* Optics Express **21**, 27338 (2013).

[24] S. Khatua, P. M. Paulo, H. Yuan, A. Gupta, P. Zijlstra, and M. Orrit, *Resonant plasmonic enhancement of single-molecule fluorescence by individual gold nanorods,* ACS Nano **8**, 4440 (2014).

[25] B. Pradhan, S. Khatua, A. Gupta, T. Aartsma, G. Canters, and M. Orrit, *Gold-nanorod-enhanced fluorescence correlation spectroscopy of fluorophores with high quantum yield in lipid bilayers,* The Journal of Physical Chemistry C **120**, 25996 (2016).

[26] B. Shuang, D. Cooper, J. N. Taylor, L. Kisley, J. Chen, W. Wang, C. B. Li, T. Komatsuzaki, and C. F. Landes, *Fast step transition and state identification (STaSI) for discrete single-molecule data analysis,* The Journal of Physical Chemistry Letters **5**, 3157 (2014).

[27] B. Pradhan, S. Khatua, A. Gupta, T. Aartsma, G. Canters, and M. Orrit, *Gold-nanorod-enhanced fluorescence correlation spectroscopy of fluorophores with high quantum yield in lipid bilayers,* The Journal of Physical Chemistry C **120**, 25996 (2016).

[28] M. Yorulmaz, S. Khatua, P. Zijlstra, A. Gaiduk, and M. Orrit, *Luminescence quantum yield of single gold nanorods,* Nano Letters **12**, 4385 (2012).

[29] A. Bard and L. Faulkner, *Electrochemical Methods: Fundamentals and Applications* (Wiley, 2000).

[30] B. S. Hoener, C. P. Byers, T. S. Heiderscheit, A. S. De Silva Indrasekara, A. Hoggard, W.-S. Chang, S. Link, and C. F. Landes, *Spectroelectrochemistry of halide anion adsorption and dissolution of single gold nanorods,* The Journal of Physical Chemistry C **120**, 20604 (2016).

[31] C. P. Byers, B. S. Hoener, W. S. Chang, M. Yorulmaz, S. Link, and C. F. Landes, *Single-particle spectroscopy reveals heterogeneity in electrochemical tuning of the localized surface plasmon,* Journal of Physical Chemistry B **118**, 14047 (2014).

[32] A. Gupta, T. J. Aartsma, and G. W. Canters, *One at a time: Intramolecular electron-transfer kinetics in small laccase observed during turnover,* Journal of the American Chemical Society **136**, 2707 (2014).

[33] S. L. Murov, I. Carmichael, and G. L. Hug, *Handbook of photochemistry* (CRC Press, 1993).

[34] S. Mowry and P. J. Ogren, *Kinetics of methylene blue reduction by ascorbic acid,* Journal of Chemical Education **76**, 970 (1999).

[35] J. R. Sutter and W. Spencer, *An equilibrium and kinetic-study of the methylene blue-ferrocyanide reaction in acid-medium,* Journal of Physical Chemistry **94**, 4116 (1990).